

# 200-years ice core bromine reconstruction at Dome C (Antarctica): observational and modelling results

F. Burgay<sup>1,2</sup>, R.P. Fernandez<sup>3</sup>, D. Segato<sup>2,4</sup>, C. Turetta<sup>2,4</sup>, C. S. Blaszcak-Boxe<sup>5</sup>, R. H. Rhodes<sup>6</sup>, C. Scharchilli<sup>7</sup>, V. Ciardini<sup>7</sup>, C. Barbante<sup>2,4</sup>, A. Saiz-Lopez<sup>8</sup> & A. Spolaor<sup>2,4\*</sup>

<sup>1</sup>Paul Scherrer Institute, Laboratory of Environmental Chemistry (LUC), 5232 Villigen PSI, Switzerland

<sup>2</sup>University Ca' Foscari of Venice, Department of Environmental Sciences, Informatics and Statistics, 30172 Venice Mestre, Italy

<sup>3</sup>Institute for Interdisciplinary Science, National Research Council (ICB-CONICET), FCEN-UNCuyo, Mendoza, 5501, Argentina

<sup>4</sup>National Research Council, Institute of Polar Sciences, 30172 Venice Mestre, Italy

<sup>5</sup>Department of Geosciences, The Pennsylvania State University, State College, PA 16803, United States

<sup>6</sup>Department of Earth Sciences, University of Cambridge, Cambridge, United Kingdom

<sup>7</sup>Laboratory of Observations And Measures for the Environment and Climate (SSPT-PROTER-OEM), ENEA, Rome, Italy

<sup>8</sup>Department of Atmospheric Chemistry and Climate, Institute of Physical Chemistry Rocasolano, CSIC, Madrid, Spain

\*Corresponding author: [andrea.spolaor@unive.it](mailto:andrea.spolaor@unive.it)

**Keywords (max 6):** bromine, ice core, sea-ice variability, Dome C (Antarctica), ozone hole

**Key points (max 3)**

- Stratospheric ozone-hole depletion has not affected bromine preservation in snow at Dome C
- Volcanic eruptions have not significantly altered the snow bromine profile at Dome C over the last 200 years
- Little seasonal sea-ice variability over the last 30 years and low sensitivity to first-year sea-ice bromine emissions at Dome C do not allow the validation of Br<sub>enr</sub> as past sea-ice proxy at this site.

## 1 **Abstract**

2 Bromine enrichment ( $\text{Br}_{\text{enr}}$ ) has been proposed as an ice core proxy for past sea-ice reconstruction.  
3 Understanding the processes that influence bromine preservation in the ice is crucial to achieve a  
4 reliable interpretation of ice core signals and to potentially relate them to past sea-ice variability. Here,  
5 we present a 210 years bromine record that sheds light on the main processes controlling bromine  
6 preservation in the snow and ice at Dome C, East Antarctic plateau. Using observations alongside a  
7 modelling approach, we demonstrate that the bromine signal is preserved at Dome C and it is not  
8 affected by the strong variations in ultraviolet radiation reaching the Antarctic plateau due to the  
9 stratospheric ozone hole. Based on this, we investigate whether the Dome C  $\text{Br}_{\text{enr}}$  record can be used as  
10 an effective tracer of past Antarctic sea-ice. Due to the limited time window covered by satellite  
11 measurements and the low sea-ice variability observed during the last 30 years in East Antarctica, we  
12 cannot fully validate  $\text{Br}_{\text{enr}}$  as an effective proxy for past sea-ice reconstructions at Dome C.

## 13 **1. Introduction**

14 Halogens play an important role in the chemistry and oxidizing capacity of the Earth's atmosphere:  
15 they take part in new particle formation processes, promote mercury oxidation, influence the budget of  
16  $\text{HO}_x$  and  $\text{NO}_x$  radicals and cause ozone depletion through efficient catalytic cycles (Saiz-Lopez and  
17 Von Glasow, 2012; Simpson et al., 2007). Volcanic eruptions (Gutmann et al., 2018) and the ocean  
18 (Parrella et al., 2012; Prados-Roman et al., 2015) represent the main natural sources of halogens to the  
19 atmosphere, releasing significant amounts of bromine (Br) and iodine (I) (Cuevas et al., 2018; Carpenter  
20 et al., 2013). In this work we focus on bromine, which has been shown to dominate halogen emissions  
21 and chemistry in the polar atmosphere through the so-called "bromine explosion events" (Pratt et al.,  
22 2013; Platt and Lehrer, 1997). These are heterogeneous autocatalytic photochemical reactions, which  
23 were first described in the Arctic boundary layer and that cause the bromine-induced ozone depletion  
24 events (Fan and Jacob, 1992; Vogt et al., 1996; Foster et al., 2001; Wennberg, 1999; Barrie et al., 1988;  
25 Kreher et al., 1997). These autocatalytic multiphase chain reactions require both acidic conditions and  
26 sunlight to produce an exponential increase in atmospheric bromine concentration, mainly as gaseous

27 BrO, Br<sub>2</sub> and HOBr (Schönhardt et al., 2012; Zhao et al., 2016; Nghiem et al., 2012). In the polar  
28 regions, the most favourable substrate (i.e. with a large bromide content) to produce such bromine  
29 explosion and ozone depletion events during springtime is the sea-salt aerosol derived from surface  
30 blowing snow deposited over first-year sea-ice (FYSI), which is characterized by acidic conditions,  
31 higher Br<sup>-</sup>/Cl<sup>-</sup> ratio (Pratt et al., 2013) and higher salinity than the snow deposited over multi-year sea-  
32 ice (MYSI) (Frey et al., 2020). Direct observations from two winter cruises in the Weddell Sea  
33 (Antarctica) and model simulation, showed that significant bromine losses take place in the aerosol  
34 phase, indicating that sea-salt aerosol debromination from salty blowing snow over sea-ice represents a  
35 relevant source of gas-phase inorganic bromine to the troposphere (Frey et al., 2020; Parrella et al.,  
36 2012; Yang et al., 2005). Note that most inorganic bromine gases present in the atmosphere are highly  
37 water-soluble and they suffer wet and dry deposition over the ice sheets (Legrand et al., 2021; Parrella  
38 et al., 2012; Fernandez et al., 2019).

39 Especially during the “bromine explosion events”, bromine, that shares the same sources as sodium  
40 (i.e. sea-salt), is significantly enriched compared to sodium (Na) in the FYSI surfaces, exceeding the  
41 bromine-to-sodium mass ratio of seawater (Millero et al., 2008). Being promoted by the presence of  
42 FYSI compared to MYSI, this bromine enrichment (Br<sub>enr</sub>, eq 1) has been proposed as a potential tracer  
43 for the reconstruction of past FYSI conditions (Spolaor et al., 2016; Maffezzoli et al., 2019; Spolaor et  
44 al., 2013b; Vallelonga et al., 2017). Qualitatively, higher Br<sub>enr</sub> values were linked to larger FYSI extent  
45 (Spolaor et al., 2013b). However, many unknowns, mainly related to the source, transport and  
46 preservation of bromine within the snowpack, still remain (Maffezzoli et al., 2019). For example, it has  
47 been suggested that the anthropogenic-induced acidity increase of the snow deposited over the sea-ice  
48 surface can enhance the sea salt debromination rates enhancing the release of reactive bromine from  
49 sea-salt aerosols into the atmosphere (Maselli et al., 2017; Sander et al., 2003). Further, bromine can  
50 also be re-emitted from the snowpack after deposition and prior to burial. However, the results obtained  
51 from previous studies are contradictory and site-specific (McConnell et al., 2017; Legrand et al., 2016;  
52 Dibb et al., 2010; Spolaor et al., 2019). In Greenland, Dibb et al., (2010) showed that bromine photo-  
53 activation was present during spring/summer and highlighted an efficient Br chemical cycling above

54 the snow. In the Svalbard Archipelago, a high-temporal resolution study designed to investigate the  
55 potential photo-emission of bromine from the snowpack (Spolaor et al., 2019) did not highlight any  
56 bromine diurnal cycle, suggesting its preservation in snow. In Antarctica, through the investigation of  
57 Na and Br fluxes against snow accumulation rate, McConnell et al., (2017) found that bromine re-  
58 emission from the Antarctic snowpack is inversely dependent on the accumulation rate. It was shown  
59 that the bromine loss from the snowpack was higher (65%) at sites with the lowest accumulation rate  
60 ( $50 \text{ kg m}^{-2} \text{ yr}^{-1}$ ), and it decreased to 11% at sites with high annual accumulation rate ( $300 \text{ kg m}^{-2} \text{ yr}^{-1}$ ).  
61 Based on these observations, virtually all bromine deposited at Dome C (Antarctica), where the annual  
62 snow accumulation is  $\approx 25\text{-}28 \text{ kg m}^{-2} \text{ yr}^{-1}$ , would have been re-emitted to the atmosphere prior to burial  
63 (McConnell et al., 2017; Maffezzoli et al., 2019). These conclusions contrast with previous observations  
64 performed at Dome C that reported no significant bromine re-emission from the snowpack (Legrand et  
65 al., 2016). An additional process that can affect bromine preservation within the snowpack has been  
66 identified in coincidence with the 17.7 ka Mt. Takahe volcanic eruption, when, the combination of an  
67 increased surface ultraviolet (UV) radiation, due to stratospheric ozone depletion, and high acidity  
68 conditions was associated with a decrease in ice bromine concentration (McConnell et al., 2017). To our  
69 knowledge, there are no investigations that focused on the effects of the modern UV-radiation changes  
70 reaching the Antarctic plateau, due to the ozone-hole formation, on bromine preservation in snow.

71 To unravel the physicochemical processes that can influence bromine preservation in the snow, we  
72 investigated the main pathways that can induce its emission from the snowpack to the atmosphere.  
73 Bromine is mainly present in the Antarctic snowpack as bromide (Spolaor et al., 2013a) and it can be  
74 oxidized by OH radicals (George and Anastasio, 2007; Abbatt et al., 2010) to form evaporable gaseous  
75 bromine. The main 'OH source within the snowpack is the photolysis of hydrogen peroxide (Chu and  
76 Anastasio, 2005), nitrate (Chu and Anastasio, 2003; Abbatt et al., 2010) and nitrite (Chu and Anastasio,  
77 2007). Understanding the relevance of each of these photochemical pathways in explaining the  
78 preservation of bromide in the Antarctic snowpack before and after the onset of the modern-ozone hole  
79 is then crucial for a reliable interpretation of the bromine enrichment profile observed in ice core  
80 records.

81 In this study, we present the first bromine record retrieved from a shallow firn core collected at  
82 Dome C, Antarctica, covering the period 1800-2012. Through the evaluation of the bromine profile, it  
83 is possible to provide new evidence about the role of the enhanced solar-UV radiation due to the onset  
84 of the modern Antarctic ozone hole (1975) on bromine preservation in the snowpack. An extended  
85 evaluation of the role of  $\text{OH}$  precursors and their relevance at Dome C is also performed. Lastly, an  
86 assessment of the suitability of  $\text{Br}_{\text{enr}}$  as a potential past sea-ice tracer at Dome C is also addressed by  
87 combining air-mass transport re-analysis and sea-ice extent satellite observations. The results presented  
88 in this paper open new perspectives on future long-term bromine studies from ice cores retrieved from  
89 low accumulation areas, aimed at forecasting future deep core drillings at Dome C, such as those  
90 planned for the Beyond EPICA project.

## 91 **2. Material and Methods**

### 92 *2.1 Ice core sampling and location*

93  
94 A 13.72 m shallow ice-core was drilled close to Concordia Station, at Dome C (3233 m a.s.l.;  
95  $75^{\circ}05'59''\text{S}$ ,  $123^{\circ}19'56''\text{E}$ ) in 2012. The retrieved shallow ice-core covers approximately 212 years,  
96 from 1800 to 2012. The ice core dating is described in details by Spolaor et al., (2021), with age  
97 uncertainties ranging from 1 year at surface to 5 years at the bottom of the core. Dome C is a suitable  
98 Antarctic site for performing photochemical studies related to the preservation of reactive elements and  
99 halides within the snowpack (Savarino et al., 2007; Cairns et al., 2021; Song et al., 2018; Spolaor et al.,  
100 2018; Spolaor et al., 2021). This location presents a low and rather constant accumulation rate ( $25.3 \pm$   
101  $1.3 \text{ kg m}^{-2} \text{ yr}^{-1}$  from 1816-1998,  $28.3 \pm 1.3 \text{ kg m}^{-2} \text{ yr}^{-1}$  from 1965-1998;  $28 \text{ kg m}^{-2} \text{ yr}^{-1}$  from 2004-2011)  
102 (Frezzotti et al., 2005; Frezzotti et al., 2013; Genthon et al., 2016), and it is located about 1000 km away  
103 from shorelines, thus not being directly affected by local coastal emissions. Matching these criteria is  
104 essential for the evaluation of the effects of modern stratospheric ozone loss due to long-lived ozone  
105 depleting substances in the potential bromine release from the snowpack.

106 The shallow ice core was collected using a hand drill (3 inches diameter); the sections were sealed  
107 in plastic containers and shipped to the Institute of Polar Sciences of the National Research Council  
108 (ISP-CNR) in Venice (Italy). The ice core sections were subsequently sampled at  $5 (\pm 1) \text{ cm}$  resolution

109 (corresponding to approx. 1 year) using a ceramic knife, rinsed with Ultra Pure Water (UPW, Elga Lab,  
110 UK) after each use. Only the central part of the core was collected into 50 mL pre-cleaned polyethylene  
111 (PE) vials for subsequent analyses, while the outer 2 cm were removed by scraping with a ceramic  
112 knife. The core samples were processed in a class 1000 inorganic clean room under a class 100 laminar-  
113 flow bench. Samples were kept at -20°C and under dark conditions until the analysis to avoid any  
114 possible photolysis reaction. Since we were only interested in the water-soluble bromine and sodium  
115 fractions and to avoid potential halogen loss (Flores et al., 2020), the analyses were conducted on melted  
116 and not acidified samples by ICP-SFMS (see 2.2). The sodium record considered in this study had some  
117 gaps from 1989 to 1997 (n=12, corresponding to 5% of the total amount of samples) that were filled  
118 with Na concentration data retrieved from two snowpits collected in 2013 and 2017, as reported in  
119 Spolaor et al., 2021.

## 120 *2.2 Instrumental analysis and cleaning procedure*

121 Total sodium and bromine concentrations were determined by ICP-SFMS following Spolaor et al.,  
122 (2016). Each analytical run started and ended with an Ultra-Pure Water (UPW) cleaning session of 3  
123 min to ensure a stable background level throughout the analysis. The external standards that were used  
124 to calibrate the analytes were prepared by diluting a 1000 ppm stock IC (ion chromatography) standard  
125 solution (TraceCERT® purity grade, Sigma-Aldrich, MO, USA). The standard concentrations ranged  
126 between 1 and 200 ng g<sup>-1</sup> for sodium and 0.05 and 0.200 ng g<sup>-1</sup> for bromine. As for the samples, the  
127 standards were not acidified. Precision and accuracy of the measurements were determined through the  
128 multiple reading of selected ice samples and external standards, respectively. The relative standard  
129 deviation (RSD %) was low for all the analytes, ranging between 3–4% for sodium and 5-7% for  
130 bromine, while accuracy, expressed as the ratio between the observed and the true values, was 105%  
131 for sodium and 92% for bromine. The instrumental limit of detection (LoD), calculated as three times  
132 the standard deviation of the blank (n = 10), was 1 ng g<sup>-1</sup> for Na and 0.05 ng g<sup>-1</sup> for Br. Bromine and  
133 sodium concentration values were used to calculate bromine enrichment (Br<sub>enr</sub>) as:

$$Br_{enr} = \frac{[Br]}{[Na]} \cdot 0.0062 \quad (\text{eq. 1})$$

134 where Br and Na are the concentrations obtained from the Dome C record and 0.0062 reflects the  
135 bromine-to-sodium mass ratio in seawater (Spolaor et al., 2013b; Millero et al., 2008).

136 All the plastic material used for sample storage and analysis was washed 5 times using UPW and  
137 filled with UPW for 1 week. Then, it was rinsed again 5 times with UPW and dried under class-100  
138 laminar flow hood before use.

### 139 *2.3 Back-trajectories calculation, satellite observations and statistical analysis*

140 Backward air mass trajectories that reach the Dome C site ( $75^{\circ}05'59''\text{S}$ ,  $123^{\circ}19'56''\text{E}$ ) were  
141 calculated to identify the most likely ocean and sea-ice areas that release bromine species to the  
142 atmosphere and that can be transported to the interior of Antarctica. Back-trajectories were obtained  
143 from the Hybrid Single-Particle Lagrangian Integrated Trajectory (HYSPLIT) model (Stein et al., 2015)  
144 using European Centre for Medium-range Weather Forecasts (ECMWF) ERA5 meteorological  
145 reanalysis (Hersbach et al., 2020). ERA5 is available on 37 pressure levels with a regular spatial grid  
146 of  $0.25^{\circ} \times 0.25^{\circ}$  at hourly temporal sampling. However, due to the huge amount of trajectories needed  
147 for this study, for computation requirements, we considered ERA5 parameters on a spatial grid of  $0.5^{\circ}$   
148  $\times 0.5^{\circ}$  every three hours and 24 pressure levels (Becagli et al., 2022). 5 days backward trajectories were  
149 calculated every 3 h at 1000, 2000 and 3000 meters above Dome C model terrain height for the period  
150 1979 – 2018. Each back trajectory was then projected on the Sea-Ice Concentration field (SIC) and the  
151 10-m wind field (still in the ECMWF ERA5 reanalysis), associating each value along the trajectory path  
152 with the nearest SIC and wind speed values. The main paths of air masses reaching Dome C were  
153 highlighted dividing the southern hemisphere in a regular  $1^{\circ} \times 1^{\circ}$  mesh and counting the total number  
154 of back trajectories points at 5 days, falling in each grid cell (i.e. the hours spent by the air mass in each  
155 grid cell). Since bromine species are emitted in the marine boundary layer (MBL) (Sander et al., 2003),  
156 source bromine areas were evaluated, selecting only the trajectory where the air mass paths lie within  
157 the MBL and over sea-ice and counting the total number of resulting points, where conditions are  
158 fulfilled, in each of the  $1^{\circ} \times 1^{\circ}$  grid cells. The height of MBL was set equal to the 900 hPa Isosurface  
159 (Lewis et al., 2004) and a value of SIC > 15% were considered in order to simulate the presence of the  
160 sea-ice cover (Becagli et al., 2022). The sea-ice concentrations used in this work are derived from

161 passive-microwave radiometers on NASA's satellites. The data are publicly available at the NASA  
162 Earth Science portal (<https://earth.gsfc.nasa.gov/>) and at the National Snow and Ice Data Center portal  
163 (<http://nsidc.org>). The sea-ice extents (in km<sup>2</sup>) are calculated as the hemispheric total as well as five  
164 regions in the Southern Ocean (Indian Ocean, Western Pacific, Ross sea, Bellingshausen and Amundsen  
165 seas and the Weddell sea).

166 The correlations computed among the different variables of this study (Na, Br, Br<sub>enr</sub>, sea-ice extent  
167 data, SAM index) were performed using a 3-year moving average. This choice takes into account both  
168 the dating error of the core ( $\approx 3$  years) and the effects of wind erosion on the age distribution of surface  
169 snow that spans over more than a year (Picard et al., 2019). To identify any abrupt change point in the  
170 records, the *findchangepts()* Matlab (Mathworks) function was used.

#### 171 2.4 CAM-CHEM model set-up

172 The wavelength-dependent solar ultraviolet (UV) radiation reaching the Antarctic plateau  
173 surface at Dome-C during the 1950-2010 period was computed using the Community Earth System  
174 Model (CESM) (Tilmes et al., 2016). The setup of the atmospheric component of the model (CAM-  
175 Chem, version 4) was identical to the one used in previous studies addressing the evolution of iodine  
176 ice core records in the Arctic (Cuevas et al., 2018) and Antarctica (Spolaor et al., 2021), and considers  
177 prescribed sea surface temperatures and sea-ice distributions following the CCMI-REFC1  
178 recommendation (Eyring et al., 2013). The CAM-Chem VSL setup includes geographically distributed  
179 and seasonally-dependent natural oceanic emissions of five bromocarbons ( $VSL^{Br} = CHBr_3, CH_2Br_2,$   
180  $CH_2BrCl, CHBrCl_2, CHBr_2Cl$ ) and four iodocarbons ( $VSL^I = CH_3I, CH_2ICl, CH_2IBr, CH_2I_2$ ), whose  
181 oceanic flux is assumed to remain constant during the whole modelling period (Ordóñez et al., 2012).  
182 The chemical scheme includes the additional inorganic chlorine and bromine contribution arising from  
183 the so-called sea-salt dehalogenation recycling occurring in the marine boundary layer and the free  
184 troposphere (Fernandez et al., 2014; Fernandez et al., 2021). The model was configured in free-running  
185 mode, with 26 vertical levels expanding from the Earth's surface to approximately 40 km (3.5 hPa in  
186 the upper stratosphere), and with a spatial resolution of 1.9° latitude by 2.5° longitude. The CAM-Chem



187 REFC1 configuration used here provides a reasonable representation of the evolution of the size and  
188 depth of the ozone hole, presenting an excellent agreement with satellite ozone observations during the  
189 modelled period (Fernandez et al., 2017; Spolaor et al., 2021).

190 Here, we compute the photolysis rate constant (J-value) of different  $\cdot\text{OH}$  precursors involved in the  
191 preservation of bromine in the snowpack following the same approach used in Spolaor et al., (2021).  
192 The molar absorptivities, quantum yields and species concentrations for hydrogen peroxide, nitrate and  
193 nitrite at Dome-C are summarized in Table 1. The modeled actinic flux reaching the Antarctic surface  
194 includes 100 bins expanding from 121 nm to 750 nm, with a spectral resolution ranging from less than  
195 1 nm in the UV to 50 nm in the visible edge. In particular, the model bandwidth within the 280-400 nm  
196 spectral range considered in this work possess a mean resolution of 4 nm. Thus, the CAM-Chem surface  
197 actinic flux for each wavelength grid was linearly interpolated into a 1 nm bandwidth, and the mean J-  
198 value during the whole sunlit period (i.e., from September 1<sup>st</sup> of a given year to February 28<sup>th</sup> of next  
199 year) was computed offline at the closest gridbox to Dome-C (74.84° S; 122.5°E; model mean altitude  
200 of 3300 m a.s.l.). The complete sunlit period (spring + summer) was selected because even when the  
201 largest changes in surface actinic flux associated with the ozone hole formation are observed during  
202 spring, the UV radiation intensity reaching the Antarctic plateau maximizes during the summer (Spolaor  
203 et al., 2021).

### 204 **3 Results and discussion**

#### 205 *3.1 Sodium, bromine and bromine enrichment profiles from the Dome C shallow core*

206 Air masses arriving at Dome C originate from a vast area that extends over the Eastern Antarctic  
207 Ocean, Ross Sea and in minimal percentage from West Antarctica. Back trajectory analyses (Figure 1)  
208 confirm that the most likely source areas of bromine and sodium emissions during the 1979-2018 period  
209 extend from the Indian Ocean sector (IO, 11%) up to the Ross Sea sector (RS, 21%), with the most  
210 likely area being the Western Pacific sector (WP, 45%), with the remaining 17% from Bellingshausen  
211 and Amundsen seas (B&AS) sector.

212 The variability in sodium concentration, a conservative tracer that does not show any post-  
213 depositional transformation, is used here to evaluate the marine contribution at Dome C (Caiazza et al.,  
214 2021). Sodium concentrations along the entire record spanned from 12 to 117 ng g<sup>-1</sup>, with an average  
215 value of 40 ± 13 ng g<sup>-1</sup>. Na profile (Figure 2) shows an increase in concentration from 1800 to 1850,  
216 followed by a long-term decreasing trend until 1994. Over the last 18 years of the record, higher sodium  
217 concentrations were recorded, suggesting an enhanced transport towards Dome C. Bromine  
218 concentration at Dome C ranges from below the LoD (0.05 ng g<sup>-1</sup>) to 0.41 ng g<sup>-1</sup>, with an average value  
219 of 0.10 ± 0.05 ng g<sup>-1</sup> along the entire record. A significant bromine increase was detected since 2004  
220 when Br concentration increased from 0.10 ± 0.05 ng g<sup>-1</sup> (pre-2004) to 0.23 ± 0.09 ng g<sup>-1</sup> (post-2004).  
221 The absence of an abrupt change of the bromine signal at the onset of the ozone hole (1975) indicates  
222 that Br is preserved in the snowpack independently on the incoming UV-radiation (see section 3.2).  
223 Sodium and bromine did not show any significant correlation ( $r = 0.06$ ,  $p$ -value = 0.20) along the entire  
224 record, suggesting different deposition velocities during transport from the coast, with sodium being  
225 deposited faster than bromine. Indeed, in the polar atmosphere, sodium is present in the aerosol phase  
226 and it is mainly affected by wet deposition processes. It was observed that its concentration decreases  
227 significantly with distance from the coast, reaching a rather constant deposition rate at approximately  
228 400 km inland (Vallelonga et al., 2021). Contrarily, bromine exists in both the aerosol and in the gas  
229 phase, its atmospheric lifetime is also driven by dry deposition processes, it can experience  
230 heterogeneous chemical recycling during transport and its concentration gradually decreases from 100  
231 km to 1000 km inland (Simpson et al., 2005; Vallelonga et al., 2021).

232 Br<sub>enr</sub> values ranged between 0.07 and 1.6 with an average value of 0.4 ± 0.3 along the entire record.  
233 Contrarily to sodium and bromine, the enrichment did not show any significant increase in the recent  
234 part of the record. On the contrary, a significant regime change was detected in 1825, when the Br<sub>enr</sub>  
235 mean value changed from 0.7 ± 0.3 (1800-1825) to 0.4 ± 0.3 (1825-2012). A two-sample  $t$ -test  
236 strengthened the significant difference between the two periods ( $p$ -value < .001). In general, Br<sub>enr</sub> values  
237 were mainly below 1 (i.e. bromine is depleted relative to sodium), which is expected at remote locations  
238 like Dome C, since the Br to Na ratio depends on the relative transport times of sea salt aerosol and

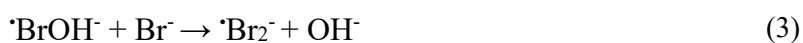
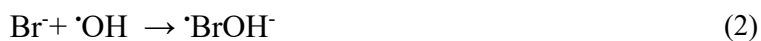
239 gaseous bromine compounds in the atmosphere (Spolaor et al., 2013b; Simpson et al., 2007; Vallelonga  
240 et al., 2021). Thus, our findings agree with the synthesis of Vallelonga et al. (2021), which show low  
241  $Br_{\text{enr}}$  values near the coast, a gradual increase at 300-600 km inland and a following decrease to values  
242 lower than 1 for all sites located more than 800 km from the coast. The few  $Br_{\text{enr}}$  values higher than 1  
243 may indicate larger FYSI surface from the source areas (Spolaor et al., 2016) or different bromine  
244 partitioning between the aerosol and gas phase that depends on the aerosol size and, consequently, on  
245 atmospheric resident times (Legrand et al., 2016; Maffezzoli et al., 2019; Vallelonga et al., 2021). In  
246 addition, changes in background atmospheric  $\cdot\text{OH}$  and  $\text{NO}_x$  might have had an impact on the gas-phase  
247 bromine partitioning between reservoir and reactive species that might have led to a faster bromine  
248 deposition since species like  $\text{BrONO}_2$  and  $\text{HOBr}$  have larger and more efficient deposition velocities  
249 than reactive species like  $\text{BrO}$  and  $\text{Br}$  (Saiz-Lopez and Fernandez, 2016; Fernandez et al., 2019).

250 In Antarctica, few other long-term bromine records exist and they were all collected from coastal  
251 sites (Spolaor et al., 2013b; Vallelonga et al., 2017). In contrast to Dome C, these records are more  
252 directly influenced by local marine contributions. The shorter atmospheric transport time from the  
253 source to the deposition location is reflected by the higher  $Br_{\text{enr}}$  values observed in these cores  
254 (Vallelonga et al., 2017).

### 255 *3.2 Bromine preservation in the snowpack at Dome C*

256 When reaching the snowpack, UV radiation can rapidly break weak chemical bonds and, due to its  
257 high energy, can promote photochemical reactions, especially in the UV-A (320–400 nm) and UV-B  
258 (290-320 nm) wavelength bands (Grannas et al., 2007). Due to its low accumulation rate, Dome C is  
259 the perfect location for performing UV-photolysis studies on chemical species occurring at the ice and  
260 snow surface (Frey et al., 2009; Savarino et al., 2007). The stratospheric ozone layer depletion observed  
261 since 1975, has caused an increase in the incoming solar UV radiation over Antarctica at  $\lambda < 300$  nm,  
262 enhancing, for example, the photochemical iodide oxidation and its subsequent release from the  
263 snowpack (Spolaor et al., 2021).

264 As highlighted in section 3.1, no significant changes neither in bromine concentration nor in  
 265 bromine enrichment have been detected at Dome C since 1975, suggesting that, contrarily to iodine  
 266 (Spolaor et al., 2021), the  $\approx 10$ -fold enhanced UV-radiation reaching the Antarctic plateau has not altered  
 267 bromine preservation within the snowpack (Figure 2). Moreover, laboratory and chamber experiments  
 268 showed enhanced photochemical oxidation and subsequent release of  $I_{2(g)}$  from artificial snow/ice and  
 269 the snowpack through the formation of a critical I-O<sub>2</sub> complex having an absorption band centred at  
 270 290 nm (Kim et al., 2016). At present, there is no evidence and/or available literature describing a  
 271 similar Br-O<sub>2</sub> complex, and/or any other brominated intermediate product, that leads then to the release  
 272 of  $Br_{2(g)}$ . In fact, the main inorganic route for bromide oxidation requires radical oxidants (e.g.  $\cdot OH$ ) to  
 273 drive the redox production of hypobromous acid (BrOH) (Artiglia et al., 2017). This oxidized species  
 274 can then combine with other reduced halide ions to form molecular halogen compounds that are released  
 275 into the gas phase (eq. 2-5) (George and Anastasio, 2007):



276 Over ice and snow substrates, hydroxyl radicals ( $\cdot OH$ ) can be produced by the photolysis of  
 277 hydrogen peroxide ( $H_2O_2$ ), nitrate ( $NO_3^-$ ) and nitrite ( $NO_2^-$ ) (Chu and Anastasio, 2005; Abbatt et al.,  
 278 2010; Chu and Anastasio, 2007). Between 290-340 nm wavelengths,  $H_2O_2$  has a wavelength-dependent  
 279 molar absorptivity that is 2.5-7.1 times lower than that for  $NO_3^-$ . Nevertheless,  $H_2O_2$  has a  $\approx 160$  times  
 280 greater quantum yield for  $\cdot OH$  production (Table 1) that is insensitive to ionic strength, pH and  
 281 wavelength (Chu and Anastasio, 2005). Therefore, for a given concentration,  $H_2O_2$  is a much more  
 282 effective source of  $\cdot OH$  than nitrate. To our knowledge, the only  $H_2O_2$  concentration value available at  
 283 Dome C is  $2 \text{ ng g}^{-1}$ , derived from a sample collected at 3.5 m-depth (Frey et al., 2006). This low value,  
 284 compared to other locations, is consistent with semi-empirical models that predict a complete hydrogen  
 285 peroxide loss when the accumulation rate is below  $\approx 70 \text{ kg m}^{-2} \text{ yr}^{-1}$  and the annual mean temperature is  
 286  $-50^\circ\text{C}$  (Frey et al., 2006). Considering that Dome C has an annual mean accumulation of  $\approx 25\text{-}28 \text{ kg m}^{-2}$

287  $^2 \text{yr}^{-1}$  (Genthon et al., 2016) and an annual mean temperature between  $-54$  and  $-50^\circ\text{C}$  (Genthon et al.,  
288 2021), we assume that the majority of the deposited or *in situ* produced  $\text{H}_2\text{O}_2$  is rapidly lost to the  
289 atmosphere.

290 Alternatively,  $\text{NO}_3^-$  photolysis (Table 1), occurring at wavelengths of 290-340 nm, with a maximum  
291 at 320 nm (Winton et al., 2020), can act as a  $\cdot\text{OH}$  source following the equations 6-9 (Chu and Anastasio,  
292 2005; Abbatt et al., 2010; Boxe, 2005):



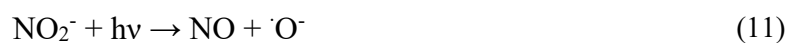
293 The  $\cdot\text{OH}$  radicals, formed by nitrate photolysis can produce  $\text{Br}_{2(\text{g})}$  following reactions 2-5. The  
294 typical snowpack nitrate profile at Dome C ranges between 22 and 147  $\text{ng g}^{-1}$  (Caiazzo et al., 2021;  
295 Spolaor et al., 2021) and shows an exponential decay in concentration with depth driven by nitrate UV-  
296 photolysis and recycling (Winton et al., 2020; Röthlisberger et al., 2000; Savarino et al., 2007). Due to  
297 its higher concentration compared with hydrogen peroxide, nitrate may represent a relevant  $\cdot\text{OH}$  source  
298 at Dome C despite its lower quantum yield for  $\cdot\text{OH}$  production. The nitrate UV-photolysis, followed by  
299  $\cdot\text{OH}$  formation and  $\text{Br}_{2(\text{g})}$  emission, has been reported under laboratory conditions with a significant  
300 dependency on the ice pH, with the largest  $\text{Br}_{2(\text{g})}$  emissions observed at low pH (George and Anastasio,  
301 2007).

302 Another source of OH radicals is nitrite (Minero et al., 2007), which can be produced by the  
303 dissociation of nitrous acid (HONO) in the condensed phase (eq. 10);



304 or by the direct formation from the minor channel (quantum yield of approximately 0.0011) of nitrate  
305 photolysis (eq. 6) (Dubowski et al., 2002).

306 Nitrite displays two major absorption bands peaking at 300 and 354 nm and, through its  
307 photolysis, it can produce  $\cdot\text{OH}$  (eq. 11-12):



308 The  $\cdot\text{OH}$  quantum yield from nitrite photo-dissociation depends both on the wavelength (increases  
309 with decreasing wavelength) and on temperature (decreases with decreasing temperature). In addition,  
310 nitrite has a  $\approx 2$ -fold higher molar absorptivity than nitrate between 280 and 300 nm (Chu and Anastasio,  
311 2007) and its  $\cdot\text{OH}$  quantum yield in ice is equal to 0.020 (at 240 K,  $\lambda = 300$ ), which is 6-fold higher than  
312 the one calculated for nitrate (Table 1). Unfortunately, there are no direct measurements of nitrite at  
313 Dome C, meaning that its concentration needs to be estimated. Following the approach used by Chu  
314 and Anastasio (2007), we assumed that at Dome C the nitrite concentration is similar to the one  
315 calculated at the South Pole, which is  $0.092 \text{ ng g}^{-1}$ . This assumption is based on: a) similar superficial  
316  $\text{NO}_3^-$  concentrations recorded both at the South Pole ( $99 \text{ ng g}^{-1}$ ) and at Dome C ( $90\text{-}147 \text{ ng g}^{-1}$ ); b) the  
317 use of  $\text{NO}_3^-$  photolysis as the main source for nitrite in the snow (Chu and Anastasio, 2007); and c) the  
318 similar total UV-radiation intensities and seasonality reaching both locations.

319 To evaluate the relevance of these processes on the OH radical production in the snow-grains and,  
320 consequently their role in promoting  $\text{Br}_{2(\text{g})}$  emission from the snowpack, we modelled the hydrogen  
321 peroxide, nitrate and nitrite photo-activation before (1950-1975) and after the ozone hole formation  
322 (post-1975) at Dome C, following the wavelength-dependent CAM-Chem model actinic flux output  
323 and the methodology described in Spolaor et al.,2021. Both  $\text{H}_2\text{O}_2$  and  $\text{NO}_3^-$  exhibited a small, but  
324 significant, enhancement on their surface photolysis (J-value) after the onset of the ozone hole ( $\approx 20\%$   
325 increase) due to the higher actinic flux reaching the surface at  $\lambda < 300 \text{ nm}$ , where most of the  $\text{H}_2\text{O}_2$   
326 absorption occurs, and to a limited extent also  $\text{NO}_3^-$  (Figure 3, 4). In contrast,  $\text{NO}_2^-$  does not show a  
327 significant trend on their J-values because both absorption bands maximize at longer wavelengths,  
328 within a spectral region that is not directly affected by the formation of the ozone hole (Figure 3,4). It  
329 is important to notice that the normalized photolysis ratio between the ozone hole period and the pre-  
330 ozone hole period, strongly depends on the wavelength range considered to compute the J-value

331 integration. For example, the ratio between the ozone hole and the pre-ozone hole periods for H<sub>2</sub>O<sub>2</sub>  
332 ranges from a minimum value of 1.2 (280-390 nm) to a maximum value larger than 5 (280-300 nm)  
333 (Figure S1). Equivalent results are obtained for the J-nitrate and J-nitrite enhancements (Figure S1),  
334 although for these species, with the strongest absorption at longer wavelengths, the upper bandwidth  
335 limit used to perform the integration should not be located at values below 310-320 nm, which result in  
336 an up to 3-fold increase on the normalized ratio during the pre-ozone hole period. For these reasons,  
337 and based on the observed molar absorptivities of each species shown in Figure 3a, our best estimate of  
338 the normalized photolysis ratio shown in Figure 4c was computed considering the following  
339 wavelengths ranges 280-378 nm for H<sub>2</sub>O<sub>2</sub>, 295-357.5 nm for NO<sub>3</sub><sup>-</sup> and 280-390 nm for NO<sub>2</sub><sup>-</sup>.

340 Taking into consideration the NO<sub>3</sub><sup>-</sup>, H<sub>2</sub>O<sub>2</sub>, and NO<sub>2</sub><sup>-</sup> concentrations at Dome C and the <sup>•</sup>OH quantum  
341 yields from their photolysis (Table 1), we observed that the rates of <sup>•</sup>OH formation especially from the  
342 photolysis of H<sub>2</sub>O<sub>2</sub> and NO<sub>3</sub><sup>-</sup> slightly increased by a factor 1.1 and 1.09 compared to the pre-ozone hole  
343 period, while for nitrite the enhancement was almost negligible (1.01). The average contribution of each  
344 of this species in producing OH radicals in the snow was the same both before and after the formation  
345 of the ozone hole that is 69% from NO<sub>3</sub><sup>-</sup>, 23% from H<sub>2</sub>O<sub>2</sub>, and 8% from NO<sub>2</sub><sup>-</sup>. Specifically, the <sup>•</sup>OH  
346 formation rates during the ozone-hole (pre-ozone hole) period from NO<sub>3</sub><sup>-</sup>, H<sub>2</sub>O<sub>2</sub> and NO<sub>2</sub><sup>-</sup> photolysis  
347 are equal to 1.14E<sup>-13</sup> (1.05E<sup>-13</sup>) M s<sup>-1</sup>, 3.80 E<sup>-13</sup> (3.47E<sup>-13</sup>) M s<sup>-1</sup> and 1.2E<sup>-14</sup> (1.2E<sup>-14</sup>) M s<sup>-1</sup>, respectively  
348 (Figure 4b). Those values are calculated by multiplying the mean photolysis rate constant for <sup>•</sup>OH  
349 formation during the ozone-hole (pre-ozone hole) period (i.e. 6.4E<sup>-8</sup> (5.9E<sup>-8</sup>) s<sup>-1</sup> for NO<sub>3</sub><sup>-</sup>, 5.9 E<sup>-6</sup> (5.36E<sup>-</sup>  
350 <sup>7</sup>) s<sup>-1</sup> for H<sub>2</sub>O<sub>2</sub> and 6.2 E<sup>-5</sup> (6.2E<sup>-6</sup>) s<sup>-1</sup> for NO<sub>2</sub><sup>-</sup>) by the estimated or real snow-grain concentration (110  
351 ng g<sup>-1</sup> or 1.77E<sup>-6</sup> M, for NO<sub>3</sub><sup>-</sup>, 2.2 ng g<sup>-1</sup>, or 6.47E<sup>-8</sup> M, for H<sub>2</sub>O<sub>2</sub> and 0.092 ng g<sup>-1</sup>, or 2E<sup>-9</sup> M, for NO<sub>2</sub><sup>-</sup>).  
352 Our results are different from those computed at Neumayer station (Chu and Anastasio, 2007), where  
353 the dominant contributor to <sup>•</sup>OH production was H<sub>2</sub>O<sub>2</sub> (2.3E<sup>-11</sup> M s<sup>-1</sup>), followed by NO<sub>3</sub><sup>-</sup> (3.9E10<sup>-13</sup> M  
354 s<sup>-1</sup>) and NO<sub>2</sub><sup>-</sup> (1.8 E10<sup>-13</sup> M s<sup>-1</sup>). Further, the <sup>•</sup>OH production rate at Dome C for H<sub>2</sub>O<sub>2</sub> is 2-orders of  
355 magnitude lower than at Neumayer station, while it is similar for NO<sub>3</sub><sup>-</sup>. The contribution of nitrite at  
356 Dome C is one order of magnitude lower than that computed at Neumayer station, where nitrite has  
357 been already considered as an insignificant source of <sup>•</sup>OH because of its very low estimated

358 concentration (Chu and Anastasio, 2007). Overall, we can conclude that the contribution of  $\text{H}_2\text{O}_2$ ,  $\text{NO}_3^-$   
359 and  $\text{NO}_2^-$  in forming OH radicals is low at Dome C both before and after the ozone hole period and their  
360 change in photolysis is unlikely to have affected bromine preservation within the snowpack. This is in  
361 agreement with previous empirical observations (Legrand et al., 2016). We then propose that bromine  
362 release into the atmosphere can be favoured only in those locations where high snow acidity (e.g. in  
363 correspondence to a volcanic horizon or at coastal sites where biogenic marine emissions can enhance  
364 snow acidification) and high concentration of  $\cdot\text{OH}$  precursors (e.g.  $\text{H}_2\text{O}_2$ ) are found.

### 365 *3.3 The role of volcanic eruptions in bromine preservation at Dome C*

366 Volcanic eruptions are a significant halogen source with the emission of large amounts of HCl, HF  
367 and HBr (Pyle and Mather, 2009). In particular, BrO formation through heterogeneous photochemical  
368 reactions was detected in a volcanic plume where local  $\text{O}_3$  destruction occurred (Von Glasow et al.,  
369 2009). However, the role of volcanic eruptions in affecting bromine concentration in ice and snow has  
370 been poorly addressed. Studies performed in the European Alps (Legrand et al., 2021) and in the West  
371 Antarctic Ice Sheet Divide (McConnell et al., 2017), showed opposite results, with recorded bromine  
372 increase and depletion in coincidence with volcanic events, respectively. The Dome C shallow core  
373 presented in this work covers a period characterized by at least seven inter-hemispherical volcanic  
374 eruptions that were identified in other snow-pits and deep cores using both  $\text{nssSO}_4^{2-}$  and Fe(II) as  
375 volcanic proxies (Castellano et al., 2005; Burgay et al., 2021; Gautier et al., 2016): Pinatubo/Cerro  
376 Hudson (1991, VEI = 6), Agung (1963, VEI = 5), Krakatua (1886, VEI = 6), Cosiguina (1835, VEI =  
377 5), Tambora (1815 = 7) and UE 1809 (1809, VEI  $\geq$  5). VEI stands for Volcanic Explosivity Index, a  
378 commonly used quantity to define the magnitude of a volcanic eruption (Newhall and Self, 1982). Its  
379 values range from 0 (Hawaiian eruption) to 8 (Ultra-Plinian eruption). In this record, we did not detect  
380 any clear fingerprint neither as bromine increase nor as depletion compared to the adjacent periods,  
381 suggesting a negligible role of volcanic eruptions in affecting the Br snow chemistry in the inland  
382 Antarctic plateau (Figure S2). Nevertheless, we highlight that, due to low snow accumulation and to  
383 strong wind erosion, not all the volcanic eruptions listed above might be present in our record. Indeed,  
384 a previous investigation that compared the sulphate signal from five ice cores drilled 1 meter apart from



385 each other at Dome C showed a bulk probability of 30% of missing volcanic events when a single core  
386 is used as the site reference (Gautier et al., 2016). Among the volcanic events embraced by our record,  
387 only Krakatua, Cosiguina and UE 1809 were observed in all the previously mentioned five replicate  
388 cores, giving us confidence that for these eruptions the volcanic fingerprint is present also in our record.  
389 However, we acknowledge that a proxy-based volcanic reconstruction is missing for our core and,  
390 considering the strong spatial variability observed at Dome C, further and more specific studies are  
391 needed to investigate the impact of large inter-hemispherical volcanic eruptions on the preservation of  
392 bromine in the snowpack.

### 393 *3.4 Can $Br_{enr}$ at Dome C be used as proxy for past sea-ice extent?*

394 Having presented evidence to demonstrate the preservation of bromine in the snowpack at Dome C  
395 and the absence of a link between our Br signal and the formation of the ozone hole, we now investigate  
396 the suitability of Dome C  $Br_{enr}$  as a proxy for past sea-ice variability. Previous studies supported the use  
397 of  $Br_{enr}$  in reconstructing past Antarctic sea-ice extent (Vallelonga et al., 2017; Spolaor et al., 2013b).  
398 However, these ice core records were retrieved at coastal sites close to local source areas, where  $Br_{enr}$   
399 values were enriched with respect to sea water mass ratio. To the contrary, due to its position, Dome  
400 C receives atmospheric signals from a vast area of the East Antarctic sector (Figure 1), which extends  
401 from the Indian Ocean to the Ross Sea, potentially giving a reconstruction of past-sea-ice extent over a  
402 broader region.

403 Our 200-year ice core record shows that  $Br_{enr}$  has an average value of  $0.4 \pm 0.3$ , meaning that it is  
404 typically depleted at Dome C. This reflects the differences in Na and Br depositions as a function of the  
405 distance from the coast, with resulting  $Br_{enr}$  values lower than 1 recorded at sites located more than 800  
406 km far from the coast (Vallelonga et al., 2021). Further, due to the low snow accumulation at this  
407 location and to the low concentrations of bromine,  $Br_{enr}$  values can be influenced by surface snow  
408 removal by wind erosion, changes in meteorological patterns and changes in wind field. For these  
409 reasons, and with the current state of knowledge, the presented bromine record should be interpreted  
410 with caution.

411 To understand the driving patterns of the Dome C record and its suitability to reconstruct past sea-  
412 ice variability, we compare the Dome C  $Br_{\text{enr}}$  record with the annual averaged Southern Annular Mode  
413 (SAM) Marshall index (Marshall, 2003), satellite observations of FYSI extent from the source areas  
414 over the period 1979-2012, and with the Law Dome methanesulphonic acid ( $MSA_{\text{LD}}$ ) profile (Curran  
415 et al., 2003) (Table 2). SAM describes the poleward/equatorward movement of the westerly winds that  
416 circle Antarctica. When these winds, known as Southern Westerly Winds (SWW), contract towards  
417 Antarctica, the SAM is in its positive phase, vice-versa it is in its negative phase. The strength of wind  
418 patterns likely influences the amount of sea salt aerosols deposited at Dome C (Crosta et al., 2021), as  
419 indicated by the positive correlation of Br and Na with SAM index (0.41 and 0.61,  $p$ -value  $< 0.01$ ,  
420 respectively). This is in agreement with recent findings that highlight a prominent northward flow  
421 during the SAM negative polarity at Dome C (Kino et al., 2021). We did not observe any correlation  
422 between the SAM index and  $Br_{\text{enr}}$  values.

423 We find that for the past decades,  $Br_{\text{enr}}$  at Dome C is mainly influenced by Br deposition, given the  
424 positive and significant correlation of  $Br_{\text{enr}}$  with total Br ( $r = 0.76$ ,  $p$ -value  $\leq 0.01$ ) and the negative  
425 correlation with Na ( $r = -0.37$ ,  $p$ -value  $\leq 0.01$ ) over the entire record (Table 2). Since gas-phase bromine  
426 is emitted in enhanced concentrations (with respect to sea-water ratio) from sea-salt aerosol derived  
427 from surface blowing snow deposited over FYSI, the  $Br_{\text{enr}}$  signal at Dome C is likely to be mainly  
428 controlled by emissions and recycling from seasonal sea-ice at the Antarctic coast rather than long-  
429 range air mass transport of sea salt aerosols (Spolaor et al., 2013b).

430 To test this hypothesis, we compared our record with FYSI extent data (Parkinson and Cavalieri,  
431 2012) during the satellite era (1979-2012) over the main source areas defined through back trajectory  
432 analysis (Figure 1). As previously stated, the large majority of the back-trajectories that reaches Dome  
433 C over the period 1979–2018 originated from the WP sector (see Section 3.1, Figure 1). However, we  
434 found significant, but weak, correlations between  $Br_{\text{enr}}$  and FYSI only with the IO sector (11% of the  
435 back-trajectory points satisfying bromine loading condition) and the RS (21%) with  $r = 0.35$  ( $p$ -value  $<$   
436  $0.1$ ) and  $r = 0.3$  ( $p$ -value  $< 0.1$ ), respectively. In contrast, the closer WP sector does not show any  
437 significant correlation with  $Br_{\text{enr}}$  (Table 2). Given the main source areas from back trajectory analysis

438 are located in the WP (45%, Figure 1), we further investigate this sector by considering the MSA record  
439 retrieved from the Law Dome ice core (hereafter MSA<sub>LD</sub>), located at a coastal site facing the WP  
440 (Curran et al., 2003). MSA<sub>LD</sub> shows a positive and significant correlation with the past sea-ice extent in  
441 the WP sector ( $r = 0.89$ ,  $p\text{-value} \leq 0.01$ ), but it does not correlate with Dome C Br<sub>enr</sub>, strengthening the  
442 idea that Dome C is influenced by a broader source area than Law Dome. Based on these findings, a  
443 possible interpretation is that the IO and RS seasonal sea-ice might have a stronger influence on the  
444 Dome C Br<sub>enr</sub> profile than WP, due to their 211% and 157% average larger FYSI extent than the one  
445 recorded in the WP (Figure S3), leading to a larger emission of reactive bromine into the atmosphere.  
446 Overall, we found a weak, but significant, correlation between the Br<sub>enr</sub> record and sea-ice extent in East  
447 Antarctica (WP+RS+IO) ( $r = 0.35$ ,  $p\text{-value} \leq 0.1$ ). Nevertheless, we need to consider that overall sea-  
448 ice extent in East Antarctica has not undergone significant changes over the last three decades, with an  
449 *inter*-annual variability of ~20%. Moreover, taking into account the observed Br<sub>enr</sub> depletion at Dome  
450 C and the difficulties in capturing relatively small sea-ice variabilities due to snow remobilization,  
451 changes in meteorological patterns and in wind fields (Vallelonga et al., 2021), we hypothesize that sea-  
452 ice extent variability observed over the last decades has not been large enough to cause a significant  
453 variability in the Br<sub>enr</sub> signal at Dome C. However, it cannot be ruled out that when longer periods which  
454 extend further back in the past are considered (e.g. glacial/interglacial transitions), Br<sub>enr</sub> variations could  
455 be used as a qualitative tracer (i.e. to identify transitions between *large* and *small* FYSI extent) for  
456 FYSI variability in East Antarctica.

#### 457 **4. Conclusions**

458 In this manuscript we presented the first long-term ice core record of bromine and bromine  
459 enrichment from Dome C (Antarctica). Based on observations and modelling results, we propose that  
460 bromine is effectively preserved within the Antarctic plateau snowpack regardless of the intensity of  
461 the incoming UV-radiation. Furthermore, we find that the change in surface UV-radiation due to ozone  
462 hole formation does not affect the contribution of H<sub>2</sub>O<sub>2</sub>, NO<sub>3</sub><sup>-</sup> and NO<sub>2</sub><sup>-</sup> to the production of OH radicals  
463 and consequently the dominant OH-driven bromide oxidation channel remains slow. We suggest that  
464 neither of these photochemical mechanisms are likely to take place at Dome C, mostly due to the low

465 concentration of  $\text{H}_2\text{O}_2$  and  $\text{NO}_2^-$  as well as the low  $\cdot\text{OH}$  quantum yield from the  $\text{NO}_3^-$  photolysis. Due  
466 to the variety of chemical reactions that can influence bromine preservation within the snowpack, we  
467 suggest the inclusion of site-specific studies to assess to what extent bromine is preserved at different  
468 specific locations, i.e. through the analysis of  $\cdot\text{OH}$  precursors ( $\text{H}_2\text{O}_2$ ,  $\text{NO}_3^-$  and  $\text{NO}_2^-$ ).

469 Finally, we provided preliminary insights on the effects of volcanic eruptions on the  
470 preservation of bromine in snow at Dome C, where we did not observe any influence on the Br record.  
471 However, due to the specific and peculiar environmental conditions at Dome C and to the lack of a  
472 proxy-based volcanic eruption reconstruction for this record, our findings are not conclusive and we  
473 encourage specific investigations on this topic. We also inquired whether  $\text{Br}_{\text{enr}}$  at Dome C can be used  
474 as a sea-ice proxy for the East Antarctic sector. Despite finding weak – but significant - correlations  
475 with the Indian Ocean and Ross Sea sectors (which are the ones presenting the largest FYSI extents) it  
476 is difficult to validate  $\text{Br}_{\text{enr}}$  as an effective proxy for past sea-ice reconstructions in East Antarctica; this  
477 is primarily due to low sea-ice variability observed during the last 30 years. Future investigations at  
478 Dome C need to focus on glacial/interglacial transitions to assess whether  $\text{Br}_{\text{enr}}$  at Dome C is somehow  
479 related to large-scale variations of sea-ice extensions.

#### 480 **Author contribution**

481 **F.B.:** conceptualization, data curation, formal analysis, investigation, methodology, visualisation,  
482 writing - original draft preparation – **R.P.F.:** data curation, formal analysis, investigation, methodology,  
483 software, visualization, writing – original draft preparation, writing – review & editing – **D.S.:** data  
484 curation, formal analysis, methodology, software, visualisation, writing – original draft preparation,  
485 writing – review & editing – **C.T.:** data curation, methodology, writing – review & editing – **C.S.B-B:**  
486 writing – review & editing – **R.H.R.:**, writing – review & editing – **C.S.:** software, writing – review &  
487 editing – **V.C.:** software, writing – review & editing – **C.B.:** funding acquisition, supervision, writing  
488 – review & editing – **A.S.L.:** investigation, writing – review & editing – **A.S.:** conceptualization,  
489 investigation, resources, supervision, writing – review & editing.

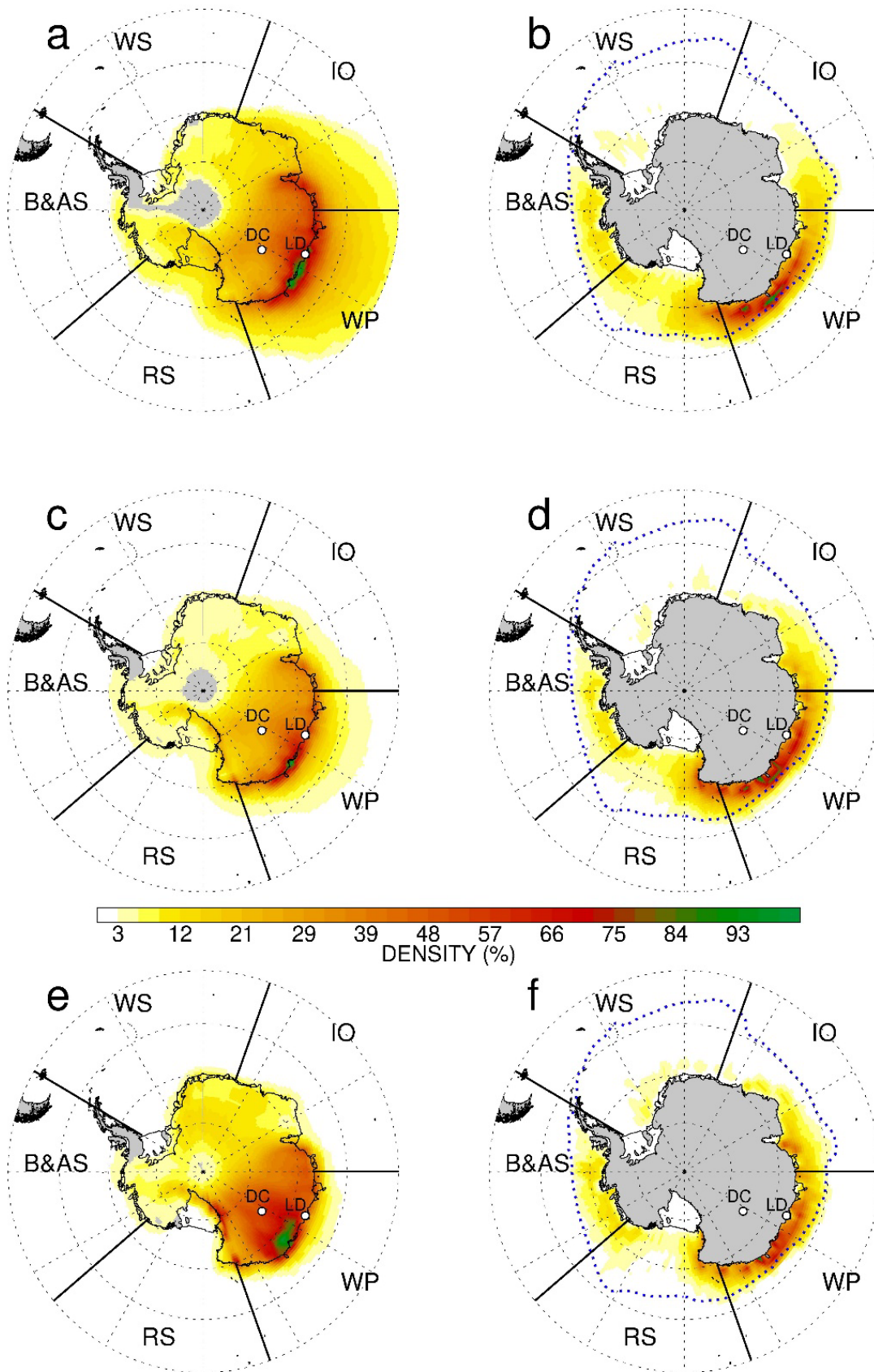
#### 490 **Acknowledgments**

491 This publication was generated in the frame of Beyond EPICA. The project has received funding from  
492 the European Union's Horizon 2020 research and innovation program under grant agreement No.  
493 815384 (Oldest Ice Core) and by the “Programma Nazionale per la Ricerca in Antartide” (PNRA,  
494 project number PNRA16\_00295). This study is also supported by the bilateral international exchange  
495 award Royal Society (UK)-CNR titled: *Antarctic sea-ice history: developing robust ice core proxies*  
496 (IEC/R2/202110) awarded to RHR and AS. Logistic support is mainly provided by PNRA and IPEV  
497 through the Concordia Station system. We acknowledge Dr. Massimo Frezzotti, for providing us  
498 physical snow data from Dome C. This is Beyond EPICA publication number XX.

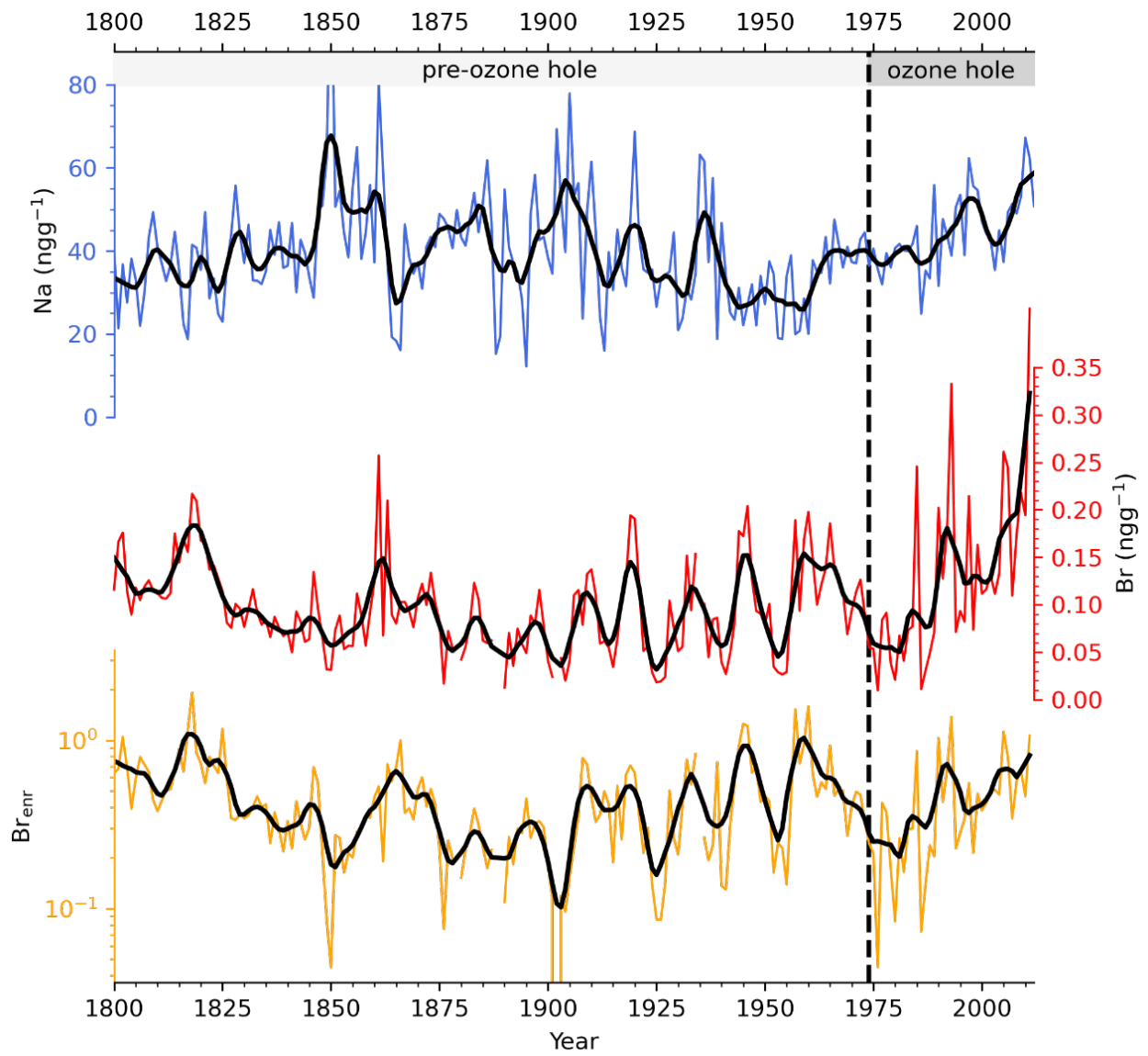
499 **Figures and Tables**

500 **Figure 1** - 5-days back-trajectory analysis of air masses arriving at the Dome C site for the period 1979-  
501 2018. The back-trajectories are calculated at (a,b) 1000 m, (c,d) 2000 m, (e,f) 3000 m above Dome C  
502 model terrain height for the period 1979-2018. Maps are divided into five sectors: Indian Ocean (IO,  
503 20°-90°), Western Pacific Ocean (WP, 90°-150°), Ross Sea (RS, 160°-230°) and Bellingshausen &  
504 Amundsen seas (B&A, 230°-20°). Panels on the left (a, c, e) represent the sum of the total number of  
505 backward trajectory points (i.e. hours) within the fifth and the second days, found in each 1° x 1° grid  
506 cell. Panels on the right (b, d, f) represent backward trajectory points (i.e. hours) within the MBL that  
507 cross areas with > 15% sea ice concentration at the given point of time. Each contour is normalized  
508 from 0 to 100 rescaling with respect to its maximum values and resampled to 0.5° x 0.5° grid mesh in  
509 order to increase readability. The gray dashed line represents the median ice edge in September  
510 (maximum extent) over the period 1979-2018.

511



513 **Figure 2** – Sodium (blue line), bromine (red line) and bromine enrichment (yellow line) ice core record  
514 from 1800 to 2012. Thick lines refer to a smoothed 3-year moving average.



515

516

517

518

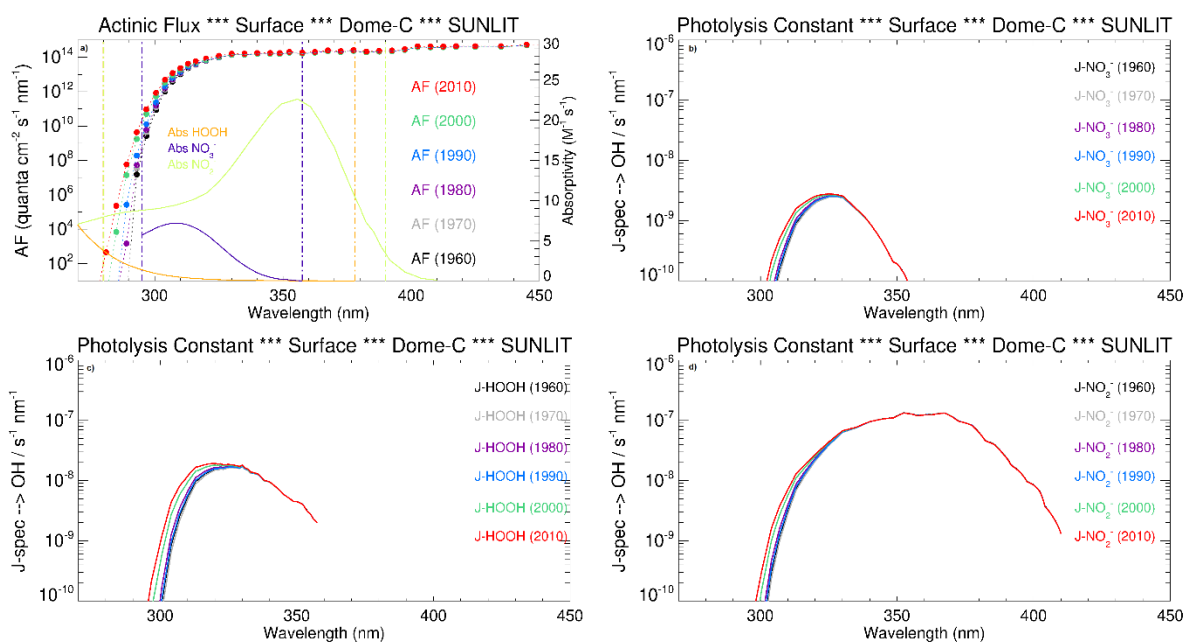
519

520



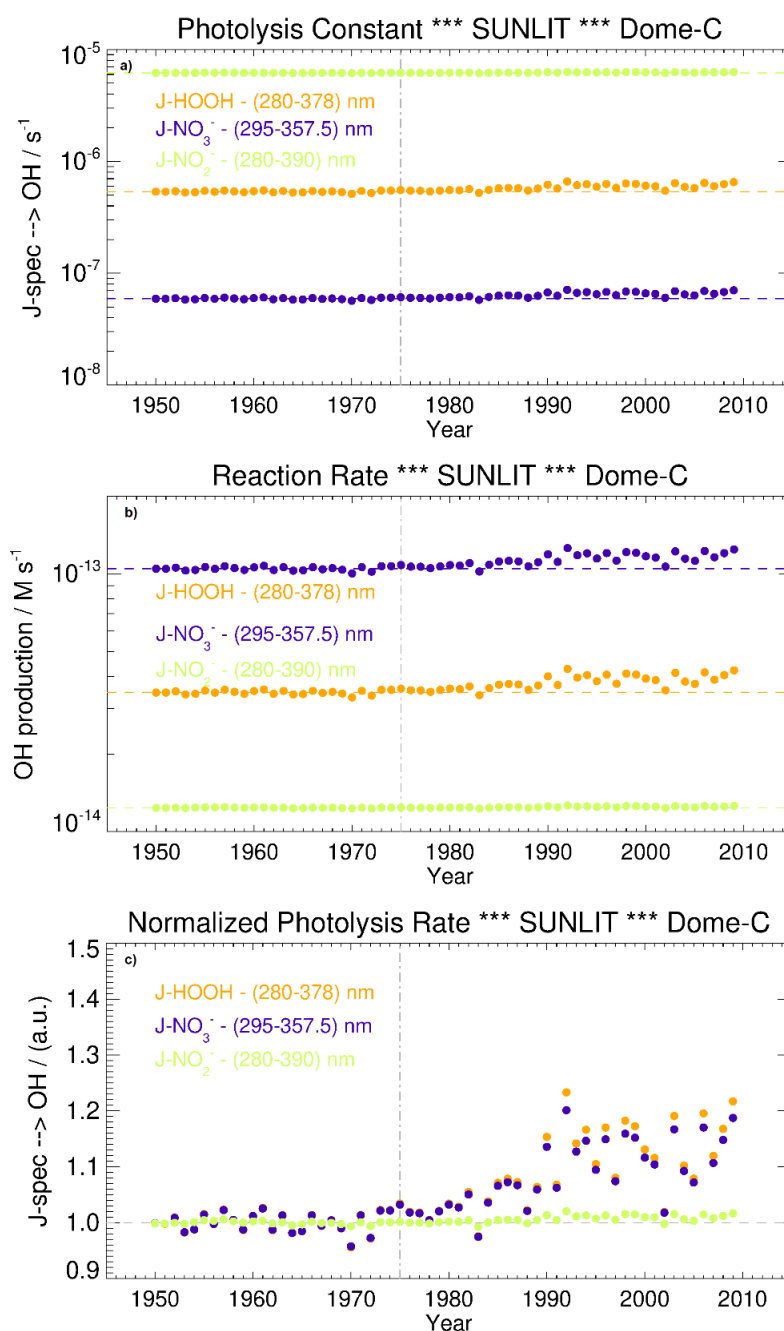
521 **Figure 3** – Panel a), the wavelength dependent actinic flux (AF) at Dome C for different years (coloured  
 522 dots), superimposed with the absorption spectrum of nitrate (violet line), hydrogen peroxide (orange  
 523 line) and nitrite (green line). The photolysis rate for the main  $\cdot\text{OH}$  precursors as a function of wavelength  
 524 in different years (pre and post the modern ozone hole) is shown for panel b) nitrate, panel c) hydrogen  
 525 peroxide and panel d) nitrite.

526



527

528 **Figure 4** – Panel a): the photolysis constant of hydrogen peroxide (orange line), nitrate (violet) and  
 529 nitrite (green) over the period 1950-2009. Panel b): the  $\cdot\text{OH}$  production rate after the hydrogen peroxide  
 530 photolysis (orange), nitrate (violet) and nitrite (green) over the period 1950-2009. Panel c): normalized  
 531 photolysis rate for hydrogen peroxide photolysis (orange line), nitrate (violet line) and nitrite (green  
 532 line) over the period 1950-2009. The dashed-grey vertical line (1975) represents the beginning of the  
 533 ozone-hole period. The horizontal-coloured lines represent the average magnitude during the pre-ozone  
 534 hole period (1950-1975).



536 **Table 1** – Summary of the  $\cdot\text{OH}$  quantum yields for  $\text{H}_2\text{O}_2$ ,  $\text{NO}_3^-$  and  $\text{NO}_2^-$ , their molar absorptivities and  
537 their concentration at Dome C. \*: estimated (more details in the text).  $\dagger$ : the value is reported from 3.5  
538 m depth.

Species	$\cdot\text{OH}$ quantum yield	Concentration at Dome C
	(Chu and Anastasio, 2007, 2005, 2003)	
$\text{H}_2\text{O}_2$	0.7	2 ng g <sup>-1</sup> (Frey et al., 2006) $\dagger$
$\text{NO}_3^-$	0.0034 at pH = 5	110 ng g <sup>-1</sup> (Spolaor et al., 2021)
$\text{NO}_2^-$	0.020 (T = 260 K, $\lambda$ = 280 nm)	0.092* ng g <sup>-1</sup>

539

540

541

542

543 **Table 2** – Pearson correlations of 3-years moving average of Dome C Br, Na and Br<sub>enr</sub>, Law Dome MSA (MSA<sub>LD</sub>) and seasonal sea-ice extents of the Indian  
544 Ocean (IO), Western Pacific (WP) and Ross Sea (RS) sectors and of the Eastern Antarctic Ocean (EAO=IO+WP+RS), calculated as  $FYSI = \overline{Extent_{Sep-Dec}} -$   
545  $Extent_{Feb}$ . The moving average is calculated in order to account for a dating error of ~ 3 years. The correlations among the chemical species (Na, Br, Br<sub>enr</sub> and  
546 NO<sub>3</sub><sup>-</sup>) were made over the entire record (1800-2012), the correlations with MSA<sub>LD</sub> were done between 1843-1995, the correlations with SAM (Marshall index)  
547 were done between 1957-2012, the correlations with sea-ice extents were done between 1979-2012. \*\*\*: p-value ≤ 0.01; \*\*: p-value ≤ 0.05; \*: p-value ≤ 0.1.

	Na	Br	Br <sub>enr</sub>	NO <sub>3</sub> <sup>-</sup>	MSA <sub>LD</sub>	SAM	IO	WP	RS	EAO
Period	1800-2012				1843-1995	1957-2012	1979-2012			
Na	1.0***	0.06	<b>-0.37***</b>	<b>0.53***</b>	-0.04	<b>0.61***</b>	0.16	-0.2	<b>0.74***</b>	<b>0.64***</b>
Br	0.06	1.0***	<b>0.76***</b>	<b>0.58***</b>	-0.05	<b>0.41***</b>	<b>0.36**</b>	-0.24	<b>0.44**</b>	<b>0.48***</b>
Br <sub>enr</sub>	<b>-0.37***</b>	<b>0.76***</b>	1.0***	<b>0.45***</b>	0.05	0.18	<b>0.35*</b>	-0.22	<b>0.3*</b>	<b>0.35*</b>
NO <sub>3</sub> <sup>-</sup>	<b>0.53***</b>	<b>0.58***</b>	<b>0.45***</b>	1.0***	0.04	0.24	0.3	-0.23	<b>0.43**</b>	<b>0.44**</b>
MSA <sub>LD</sub>	-0.04	-0.05	0.05	0.04	1.0***	-0.08	-0.13	<b>0.89***</b>	0.32	<b>0.58**</b>
SAM	<b>0.61***</b>	<b>0.41***</b>	0.18	0.24	-0.08	1.0***	0.28	-0.14	<b>0.58***</b>	<b>0.58***</b>
IO	0.16	<b>0.36**</b>	<b>0.35*</b>	0.3	-0.13	0.28	1.0***	0.0	-0.06	<b>0.42**</b>
WP	-0.2	-0.24	-0.22	-0.23	<b>0.89***</b>	-0.14	0	1.0***	-0.03	<b>0.31*</b>
RS	<b>0.74***</b>	<b>0.44**</b>	<b>0.3*</b>	<b>0.43**</b>	0.32	<b>0.58***</b>	-0.06	-0.03	1.0***	<b>0.82***</b>
EAO	<b>0.64***</b>	<b>0.48***</b>	<b>0.35*</b>	<b>0.44**</b>	<b>0.58**</b>	<b>0.58***</b>	<b>0.42**</b>	<b>0.31*</b>	<b>0.82***</b>	1.0***

- 550 Abbatt, J., Oldridge, N., Symington, A., Chukalovskiy, V., McWhinney, R., Sjostedt, S., and Cox, R.:  
551 Release of gas-phase halogens by photolytic generation of OH in frozen halide–nitrate solutions: an  
552 active halogen formation mechanism?, *The Journal of Physical Chemistry A*, 114, 6527–6533, 2010.
- 553 Artiglia, L., Edebeli, J., Orlando, F., Chen, S., Lee, M.-T., Arroyo, P. C., Gilgen, A., Bartels-Rausch,  
554 T., Kleibert, A., and Vazdar, M.: A surface-stabilized ozonide triggers bromide oxidation at the  
555 aqueous solution-vapour interface, *Nature communications*, 8, 1–8, 2017.
- 556 Barrie, L., Bottenheim, J., Schnell, R., Crutzen, P., and Rasmussen, R.: Ozone destruction and  
557 photochemical reactions at polar sunrise in the lower Arctic atmosphere, *Nature*, 334, 138–141, 1988.
- 558 Becagli, S., Marchese, C., Caiazzo, L., Ciardini, V., Lazzara, L., Mori, G., Nuccio, C., Scarchilli, C.,  
559 Severi, M., and Traversi, R.: Biogenic aerosol in central East Antarctic Plateau as a proxy for the  
560 ocean-atmosphere interaction in the Southern Ocean, *Science of The Total Environment*, 810,  
561 151285, 2022.
- 562 Boxe, C.: Nitrate photochemistry and interrelated chemical phenomena in ice, California Institute of  
563 Technology 2005.
- 564 Burgay, F., Barbaro, E., Cappelletti, D., Turetta, C., Gallet, J.-C., Isaksson, E., Stenni, B., Dreossi, G.,  
565 Scoto, F., and Barbante, C.: First discrete iron (II) records from Dome C (Antarctica) and the  
566 Holtedahlfonna glacier (Svalbard), *Chemosphere*, 267, 129335, 2021.
- 567 Caiazzo, L., Becagli, S., Bertinetti, S., Grotti, M., Nava, S., Severi, M., and Traversi, R.: High  
568 Resolution Chemical Stratigraphies of Atmospheric Depositions from a 4 m Depth Snow Pit at Dome  
569 C (East Antarctica), *Atmosphere*, 12, 909, 2021.
- 570 Cairns, W. R., Turetta, C., Maffezzoli, N., Magand, O., Araujo, B. F., Angot, H., Segato, D.,  
571 Cristofanelli, P., Sprovieri, F., and Scarchilli, C.: Mercury in precipitated and surface snow at Dome C  
572 and a first estimate of mercury depositional fluxes during the Austral summer on the high Antarctic  
573 plateau, *Atmospheric Environment*, 262, 118634, 2021.
- 574 Carpenter, L. J., MacDonald, S. M., Shaw, M. D., Kumar, R., Saunders, R. W., Parthipan, R., Wilson,  
575 J., and Plane, J. M.: Atmospheric iodine levels influenced by sea surface emissions of inorganic  
576 iodine, *Nature Geoscience*, 6, 108–111, 2013.
- 577 Castellano, E., Becagli, S., Hansson, M., Hutterli, M., Petit, J., Rampino, M., Severi, M., Steffensen,  
578 J. P., Traversi, R., and Udisti, R.: Holocene volcanic history as recorded in the sulfate stratigraphy of  
579 the European Project for Ice Coring in Antarctica Dome C (EDC96) ice core, *Journal of Geophysical  
580 Research: Atmospheres*, 110, 2005.
- 581 Chu, L. and Anastasio, C.: Quantum yields of hydroxyl radical and nitrogen dioxide from the  
582 photolysis of nitrate on ice, *The Journal of Physical Chemistry A*, 107, 9594–9602, 2003.
- 583 Chu, L. and Anastasio, C.: Formation of hydroxyl radical from the photolysis of frozen hydrogen  
584 peroxide, *The Journal of Physical Chemistry A*, 109, 6264–6271, 2005.
- 585 Chu, L. and Anastasio, C.: Temperature and wavelength dependence of nitrite photolysis in frozen  
586 and aqueous solutions, *Environmental science & technology*, 41, 3626–3632, 2007.
- 587 Crosta, X., Etourneau, J., Orme, L. C., Dalaiden, Q., Campagne, P., Swingedouw, D., Goosse, H.,  
588 Massé, G., Miettinen, A., and McKay, R. M.: Multi-decadal trends in Antarctic sea-ice extent driven  
589 by ENSO–SAM over the last 2,000 years, *Nature Geoscience*, 14, 156–160, 2021.
- 590 Cuevas, C. A., Maffezzoli, N., Corella, J. P., Spolaor, A., Vallelonga, P., Kjær, H. A., Simonsen, M.,  
591 Winstrup, M., Vinther, B., and Horvat, C.: Rapid increase in atmospheric iodine levels in the North  
592 Atlantic since the mid-20th century, *Nature communications*, 9, 1–6, 2018.
- 593 Curran, M. A., van Ommen, T. D., Morgan, V. I., Phillips, K. L., and Palmer, A. S.: Ice core evidence  
594 for Antarctic sea ice decline since the 1950s, *Science*, 302, 1203–1206, 2003.
- 595 Dibb, J. E., Ziemba, L. D., Luxford, J., and Beckman, P.: Bromide and other ions in the snow, firn air,  
596 and atmospheric boundary layer at Summit during GSHOX, *Atmospheric Chemistry and Physics*, 10,  
597 9931–9942, 2010.
- 598 Dubowski, Y., Colussi, A., Boxe, C., and Hoffmann, M.: Monotonic increase of nitrite yields in the  
599 photolysis of nitrate in ice and water between 238 and 294 K, *The Journal of Physical Chemistry A*,  
600 106, 6967–6971, 2002.

601 Eyring, V., Lamarque, J.-F., Hess, P., Arfeuille, F., Bowman, K., Chipperfield, M. P., Duncan, B.,  
602 Fiore, A., Gettelman, A., and Giorgetta, M. A.: Overview of IGAC/SPARC Chemistry-Climate Model  
603 Initiative (CCMI) community simulations in support of upcoming ozone and climate assessments,  
604 SPARC newsletter, 40, 48-66, 2013.

605 Fan, S.-M. and Jacob, D. J.: Surface ozone depletion in Arctic spring sustained by bromine reactions  
606 on aerosols, *Nature*, 359, 522-524, 1992.

607 Fernandez, R. P., Kinnison, D. E., Lamarque, J.-F., Tilmes, S., and Saiz-Lopez, A.: Impact of  
608 biogenic very short-lived bromine on the Antarctic ozone hole during the 21st century, *Atmospheric  
609 Chemistry and Physics*, 17, 1673-1688, 2017.

610 Fernandez, R. P., Salawitch, R., Kinnison, D., Lamarque, J.-F., and Saiz-Lopez, A.: Bromine  
611 partitioning in the tropical tropopause layer: implications for stratospheric injection, *Atmospheric  
612 Chemistry and Physics*, 14, 13391-13410, 2014.

613 Fernandez, R. P., Barrera, J. A., López-Noreña, A. I., Kinnison, D. E., Nicely, J., Salawitch, R. J.,  
614 Wales, P. A., Toselli, B. M., Tilmes, S., and Lamarque, J. F.: Intercomparison Between Surrogate,  
615 Explicit, and Full Treatments of VSL Bromine Chemistry Within the CAM-Chem Chemistry-Climate  
616 Model, *Geophysical research letters*, 48, e2020GL091125, 2021.

617 Fernandez, R. P., Carmona-Balea, A., Cuevas, C. A., Barrera, J. A., Kinnison, D. E., Lamarque, J. F.,  
618 Blaszcak-Boxe, C., Kim, K., Choi, W., and Hay, T.: Modeling the sources and chemistry of polar  
619 tropospheric halogens (Cl, Br, and I) using the CAM-Chem Global Chemistry-Climate Model, *Journal  
620 of Advances in Modeling Earth Systems*, 11, 2259-2289, 2019.

621 Flores, E. M., Mello, P. A., Krzyzaniak, S. R., Cauduro, V. H., and Picoloto, R. S.: Challenges and  
622 trends for halogen determination by inductively coupled plasma mass spectrometry: a review, *Rapid  
623 Communications in Mass Spectrometry*, 34, e8727, 2020.

624 Foster, K. L., Plastridge, R. A., Bottenheim, J. W., Shepson, P. B., Finlayson-Pitts, B. J., and Spicer,  
625 C. W.: The role of Br<sub>2</sub> and BrCl in surface ozone destruction at polar sunrise, *Science*, 291, 471-474,  
626 2001.

627 Frey, M. M., Bales, R. C., and McConnell, J. R.: Climate sensitivity of the century-scale hydrogen  
628 peroxide (H<sub>2</sub>O<sub>2</sub>) record preserved in 23 ice cores from West Antarctica, *Journal of Geophysical  
629 Research: Atmospheres*, 111, 2006.

630 Frey, M. M., Savarino, J., Morin, S., Erbland, J., and Martins, J.: Photolysis imprint in the nitrate  
631 stable isotope signal in snow and atmosphere of East Antarctica and implications for reactive nitrogen  
632 cycling, *Atmospheric Chemistry and Physics*, 9, 8681-8696, 2009.

633 Frey, M. M., Norris, S. J., Brooks, I. M., Anderson, P. S., Nishimura, K., Yang, X., Jones, A. E.,  
634 Nerentorp Mastromonaco, M. G., Jones, D. H., and Wolff, E. W.: First direct observation of sea salt  
635 aerosol production from blowing snow above sea ice, *Atmospheric Chemistry and Physics*, 20, 2549-  
636 2578, 2020.

637 Frezzotti, M., Scarchilli, C., Becagli, S., Proposito, M., and Urbini, S.: A synthesis of the Antarctic  
638 surface mass balance during the last 800 yr, *The Cryosphere*, 7, 303-319, 2013.

639 Frezzotti, M., Pourchet, M., Flora, O., Gandolfi, S., Gay, M., Urbini, S., Vincent, C., Becagli, S.,  
640 Gragnani, R., Proposito, M., Severi, M., Traversi, R., Udisti, R., and Fily, M.: Spatial and temporal  
641 variability of snow accumulation in East Antarctica from traverse data, *J Glaciol*, 51, 113-124,  
642 10.3189/172756505781829502, 2005.

643 Gautier, E., Savarino, J., Erbland, J., Lanciki, A., and Possenti, P.: Variability of sulfate signal in ice  
644 core records based on five replicate cores, *Climate of the Past*, 12, 103-113, 2016.

645 Genthon, C., Six, D., Scarchilli, C., Ciardini, V., and Frezzotti, M.: Meteorological and snow  
646 accumulation gradients across Dome C, East Antarctic plateau, *International Journal of Climatology*,  
647 36, 455-466, 2016.

648 Genthon, C., Veron, D., Vignon, E., Six, D., Dufresne, J.-L., Madeleine, J.-B., Sultan, E., and Forget,  
649 F.: 10 years of temperature and wind observation on a 45 m tower at Dome C, East Antarctic plateau,  
650 *Earth System Science Data*, 13, 5731-5746, 2021.

651 George, I. J. and Anastasio, C.: Release of gaseous bromine from the photolysis of nitrate and  
652 hydrogen peroxide in simulated sea-salt solutions, *Atmospheric Environment*, 41, 543-553, 2007.

653 Grannas, A., Jones, A. E., Dibb, J., Ammann, M., Anastasio, C., Beine, H., Bergin, M., Bottenheim,  
654 J., Boxe, C., and Carver, G.: An overview of snow photochemistry: evidence, mechanisms and  
655 impacts, *Atmospheric chemistry and physics*, 7, 4329-4373, 2007.

656 Gutmann, A., Bobrowski, N., Roberts, T. J., Rüdiger, J., and Hoffmann, T.: Advances in bromine  
657 speciation in volcanic plumes, *Frontiers in Earth Science*, 6, 213, 2018.

658 Hersbach, H., Bell, B., Berrisford, P., Hirahara, S., Horányi, A., Muñoz-Sabater, J., Nicolas, J.,  
659 Peubey, C., Radu, R., and Schepers, D.: The ERA5 global reanalysis, *Quarterly Journal of the Royal*  
660 *Meteorological Society*, 146, 1999-2049, 2020.

661 Kim, K., Yabushita, A., Okumura, M., Saiz-Lopez, A., Cuevas, C. A., Blaszcak-Boxe, C. S., Min, D.  
662 W., Yoon, H.-I., and Choi, W.: Production of molecular iodine and tri-iodide in the frozen solution of  
663 iodide: implication for polar atmosphere, *Environmental science & technology*, 50, 1280-1287, 2016.

664 Kino, K., Okazaki, A., Cauquoin, A., and Yoshimura, K.: Contribution of the Southern Annular Mode  
665 to variations in water isotopes of daily precipitation at Dome Fuji, East Antarctica, *Journal of*  
666 *Geophysical Research: Atmospheres*, 126, e2021JD035397, 2021.

667 Kreher, K., Johnston, P., Wood, S., Nardi, B., and Platt, U.: Ground-based measurements of  
668 tropospheric and stratospheric BrO at Arrival Heights, Antarctica, *Geophysical Research Letters*, 24,  
669 3021-3024, 1997.

670 Legrand, M., Yang, X., Preunkert, S., and Theys, N.: Year-round records of sea salt, gaseous, and  
671 particulate inorganic bromine in the atmospheric boundary layer at coastal (Dumont d'Urville) and  
672 central (Concordia) East Antarctic sites, *Journal of geophysical research: atmospheres*, 121, 997-1023,  
673 2016.

674 Legrand, M., McConnell, J., Preunkert, S., Chellman, N., and Arienzo, M.: Causes of enhanced  
675 bromine levels in Alpine ice cores during the 20th century: Implications for bromine in the free  
676 European troposphere, *Journal of Geophysical Research: Atmospheres*, 126, e2020JD034246, 2021.

677 Lewis, E. R., Lewis, R., Lewis, E. R., and Schwartz, S. E.: Sea salt aerosol production: mechanisms,  
678 methods, measurements, and models, *American geophysical union*2004.

679 Maffezzoli, N., Vallelonga, P., Edwards, R., Saiz-Lopez, A., Turetta, C., Kjær, H. A., Barbante, C.,  
680 Vinther, B., and Spolaor, A.: A 120 000-year record of sea ice in the North Atlantic?, *Climate of the*  
681 *Past*, 15, 2031-2051, 2019.

682 Marshall, G. J.: Trends in the Southern Annular Mode from observations and reanalyses, *Journal of*  
683 *climate*, 16, 4134-4143, 2003.

684 Maselli, O. J., Chellman, N. J., Grieman, M., Layman, L., McConnell, J. R., Pasteris, D., Rhodes, R.  
685 H., Saltzman, E., and Sigl, M.: Sea ice and pollution-modulated changes in Greenland ice core  
686 methanesulfonate and bromine, *Climate of the Past*, 13, 39-59, 2017.

687 McConnell, J. R., Burke, A., Dunbar, N. W., Köhler, P., Thomas, J. L., Arienzo, M. M., Chellman, N.  
688 J., Maselli, O. J., Sigl, M., and Adkins, J. F.: Synchronous volcanic eruptions and abrupt climate  
689 change~ 17.7 ka plausibly linked by stratospheric ozone depletion, *Proceedings of the National*  
690 *Academy of Sciences*, 114, 10035-10040, 2017.

691 Millero, F. J., Feistel, R., Wright, D. G., and McDougall, T. J.: The composition of Standard Seawater  
692 and the definition of the Reference-Composition Salinity Scale, *Deep Sea Research Part I:*  
693 *Oceanographic Research Papers*, 55, 50-72, 2008.

694 Minero, C., Chiron, S., Falletti, G., Maurino, V., Pelizzetti, E., Ajassa, R., Carlotti, M. E., and Vione,  
695 D.: Photochemical processes involving nitrite in surface water samples, *Aquatic Sciences*, 69, 71-85,  
696 2007.

697 Newhall, C. G. and Self, S.: The volcanic explosivity index (VEI) an estimate of explosive magnitude  
698 for historical volcanism, *Journal of Geophysical Research: Oceans*, 87, 1231-1238, 1982.

699 Nghiem, S. V., Rigor, I. G., Richter, A., Burrows, J. P., Shepson, P. B., Bottenheim, J., Barber, D. G.,  
700 Steffen, A., Latonas, J., and Wang, F.: Field and satellite observations of the formation and  
701 distribution of Arctic atmospheric bromine above a rejuvenated sea ice cover, *Journal of Geophysical*  
702 *Research: Atmospheres*, 117, 2012.

703 Ordóñez, C., Lamarque, J.-F., Tilmes, S., Kinnison, D. E., Atlas, E. L., Blake, D. R., Sousa Santos,  
704 G., Brasseur, G., and Saiz-Lopez, A.: Bromine and iodine chemistry in a global chemistry-climate  
705 model: description and evaluation of very short-lived oceanic sources, *Atmospheric Chemistry and*  
706 *Physics*, 12, 1423-1447, 2012.

707 Parkinson, C. L. and Cavalieri, D. J.: Antarctic sea ice variability and trends, 1979–2010, *The*  
708 *Cryosphere*, 6, 871-880, 2012.

709 Parrella, J., Jacob, D. J., Liang, Q., Zhang, Y., Mickley, L. J., Miller, B., Evans, M., Yang, X., Pyle,  
710 J., and Theys, N.: Tropospheric bromine chemistry: implications for present and pre-industrial ozone  
711 and mercury, *Atmospheric Chemistry and Physics*, 12, 6723-6740, 2012.

712 Picard, G., Arnaud, L., Caneill, R., Lefebvre, E., and Lamare, M.: Observation of the process of snow  
713 accumulation on the Antarctic Plateau by time lapse laser scanning, *The Cryosphere*, 13, 1983-1999,  
714 2019.

715 Platt, U. and Lehrer, E.: ARCTOC Final Report to the European Union, 1997.

716 Prados-Roman, C., Cuevas, C. A., Fernandez, R. P., Kinnison, D. E., Lamarque, J. F., and Saiz-  
717 Lopez, A.: A negative feedback between anthropogenic ozone pollution and enhanced ocean  
718 emissions of iodine, *Atmospheric Chemistry and Physics*, 15, 2215-2224, 2015.

719 Pratt, K. A., Custard, K. D., Shepson, P. B., Douglas, T. A., Pöhler, D., General, S., Zielcke, J.,  
720 Simpson, W. R., Platt, U., and Tanner, D. J.: Photochemical production of molecular bromine in  
721 Arctic surface snowpacks, *Nature Geoscience*, 6, 351-356, 2013.

722 Pyle, D. and Mather, T.: Halogens in igneous processes and their fluxes to the atmosphere and oceans  
723 from volcanic activity: A review, *Chemical Geology*, 263, 110-121, 2009.

724 Röthlisberger, R., Hutterli, M. A., Sommer, S., Wolff, E. W., and Mulvaney, R.: Factors controlling  
725 nitrate in ice cores: Evidence from the Dome C deep ice core, *Journal of Geophysical Research:*  
726 *Atmospheres*, 105, 20565-20572, 2000.

727 Saiz-Lopez, A. and von Glasow, R.: Reactive halogen chemistry in the troposphere, *Chemical Society*  
728 *Reviews*, 41, 6448-6472, 2012.

729 Saiz-Lopez, A. and Fernandez, R. P.: On the formation of tropical rings of atomic halogens: Causes  
730 and implications, *Geophysical Research Letters*, 43, 2928-2935, 2016.

731 Sander, R., Keene, W., Pszenny, A., Arimoto, R., Ayers, G., Baboukas, E., Cainey, J., Crutzen, P.,  
732 Duce, R., and Hönninger, G.: Inorganic bromine in the marine boundary layer: a critical review,  
733 *Atmospheric Chemistry and Physics*, 3, 1301-1336, 2003.

734 Savarino, J., Kaiser, J., Morin, S., Sigman, D. M., and Thiemens, M.: Nitrogen and oxygen isotopic  
735 constraints on the origin of atmospheric nitrate in coastal Antarctica, *Atmospheric Chemistry and*  
736 *Physics*, 7, 1925-1945, 2007.

737 Schönhardt, A., Begoin, M., Richter, A., Wittrock, F., Kaleschke, L., Gómez Martín, J., and Burrows,  
738 J.: Simultaneous satellite observations of IO and BrO over Antarctica, *Atmospheric Chemistry and*  
739 *Physics*, 12, 6565-6580, 2012.

740 Simpson, W. R., Alvarez-Aviles, L., Douglas, T. A., Sturm, M., and Domine, F.: Halogens in the  
741 coastal snow pack near Barrow, Alaska: Evidence for active bromine air-snow chemistry during  
742 springtime, *Geophysical research letters*, 32, 2005.

743 Simpson, W. R., Glasow, R. v., Riedel, K., Anderson, P., Ariya, P., Bottenheim, J., Burrows, J.,  
744 Carpenter, L., Frieß, U., and Goodsite, M. E.: Halogens and their role in polar boundary-layer ozone  
745 depletion, *Atmospheric Chemistry and Physics*, 7, 4375-4418, 2007.

746 Song, S., Angot, H., Selin, N. E., Gallée, H., Sprovieri, F., Pirrone, N., Helmig, D., Savarino, J.,  
747 Magand, O., and Dommergue, A.: Understanding mercury oxidation and air-snow exchange on the  
748 East Antarctic Plateau: a modeling study, *Atmospheric Chemistry and Physics*, 18, 15825-15840,  
749 2018.

750 Spolaor, A., Angot, H., Roman, M., Dommergue, A., Scarchilli, C., Vardè, M., Del Guasta, M.,  
751 Pedeli, X., Varin, C., and Sprovieri, F.: Feedback mechanisms between snow and atmospheric  
752 mercury: Results and observations from field campaigns on the Antarctic plateau, *Chemosphere*, 197,  
753 306-317, 2018.

754 Spolaor, A., Barbaro, E., Cappelletti, D., Turetta, C., Mazzola, M., Giardi, F., Björkman, M. P.,  
755 Lucchetta, F., Dallo, F., and Aspö Pfaffhuber, K.: Diurnal cycle of iodine, bromine, and mercury  
756 concentrations in Svalbard surface snow, 2019.

757 Spolaor, A., Vallenga, P., Gabrieli, J., Kehrwald, N., Turetta, C., Cozzi, G., Poto, L., Plane, J.,  
758 Boutron, C., and Barbante, C.: Speciation analysis of iodine and bromine at picogram-per-gram levels  
759 in polar ice, *Analytical and bioanalytical chemistry*, 405, 647-654, 2013a.

760 Spolaor, A., Vallenga, P., Plane, J., Kehrwald, N., Gabrieli, J., Varin, C., Turetta, C., Cozzi, G.,  
761 Kumar, R., and Boutron, C.: Halogen species record Antarctic sea ice extent over glacial-interglacial  
762 periods, *Atmospheric Chemistry and Physics*, 13, 6623-6635, 2013b.



763 Spolaor, A., Vallelonga, P., Turetta, C., Maffezzoli, N., Cozzi, G., Gabrieli, J., Barbante, C., Goto-  
764 Azuma, K., Saiz-Lopez, A., Cuevas, C. A., and Dahl-Jensen, D.: Canadian Arctic sea ice  
765 reconstructed from bromine in the Greenland NEEM ice core, *Scientific Reports*, 6, 33925,  
766 10.1038/srep33925, 2016.

767 Spolaor, A., Burgay, F., Fernandez, R. P., Turetta, C., Cuevas, C. A., Kim, K., Kinnison, D. E.,  
768 Lamarque, J.-F., de Blasi, F., Barbaro, E., Corella, J. P., Vallelonga, P., Frezzotti, M., Barbante, C.,  
769 and Saiz-Lopez, A.: Antarctic ozone hole modifies iodine geochemistry on the Antarctic Plateau,  
770 *Nature Communications*, 12, 5836, 10.1038/s41467-021-26109-x, 2021.

771 Stein, A., Draxler, R. R., Rolph, G. D., Stunder, B. J., Cohen, M., and Ngan, F.: NOAA's HYSPLIT  
772 atmospheric transport and dispersion modeling system, *Bulletin of the American Meteorological*  
773 *Society*, 96, 2059-2077, 2015.

774 Tilmes, S., Lamarque, J.-F., Emmons, L. K., Kinnison, D. E., Marsh, D., Garcia, R. R., Smith, A. K.,  
775 Neely, R. R., Conley, A., and Vitt, F.: Representation of the community earth system model (CESM1)  
776 CAM4-chem within the chemistry-climate model initiative (CCMI), *Geoscientific Model*  
777 *Development*, 9, 1853-1890, 2016.

778 Vallelonga, P., Maffezzoli, N., Saiz-Lopez, A., Scoto, F., Kjær, H. A., and Spolaor, A.: Sea-ice  
779 reconstructions from bromine and iodine in ice cores, *Quaternary Science Reviews*, 269, 107133,  
780 2021.

781 Vallelonga, P., Maffezzoli, N., Moy, A. D., Curran, M. A., Vance, T. R., Edwards, R., Hughes, G.,  
782 Barker, E., Spreen, G., and Saiz-Lopez, A.: Sea-ice-related halogen enrichment at Law Dome, coastal  
783 East Antarctica, *Climate of the Past*, 13, 171-184, 2017.

784 Vogt, R., Crutzen, P. J., and Sander, R.: A mechanism for halogen release from sea-salt aerosol in the  
785 remote marine boundary layer, *Nature*, 383, 327-330, 1996.

786 von Glasow, R., Bobrowski, N., and Kern, C.: The effects of volcanic eruptions on atmospheric  
787 chemistry, *Chemical Geology*, 263, 131-142, 2009.

788 Wennberg, P.: Bromine explosion, *Nature*, 397, 299-301, 1999.

789 Winton, V. H. L., Ming, A., Caillon, N., Hauge, L., Jones, A. E., Savarino, J., Yang, X., and Frey, M.  
790 M.: Deposition, recycling, and archival of nitrate stable isotopes between the air-snow interface:  
791 comparison between Dronning Maud Land and Dome C, Antarctica, *Atmospheric Chemistry and*  
792 *Physics*, 20, 5861-5885, 2020.

793 Yang, X., Cox, R. A., Warwick, N. J., Pyle, J. A., Carver, G. D., O'Connor, F. M., and Savage, N. H.:  
794 Tropospheric bromine chemistry and its impacts on ozone: A model study, *Journal of Geophysical*  
795 *Research: Atmospheres*, 110, 2005.

796 Zhao, X., Strong, K., Adams, C., Schofield, R., Yang, X., Richter, A., Friess, U., Blechschmidt, A.  
797 M., and Koo, J. H.: A case study of a transported bromine explosion event in the Canadian high arctic,  
798 *Journal of Geophysical Research: Atmospheres*, 121, 457-477, 2016.

799